Environmental Earth Sciences (2021) 80:714
https://doi.org/10.1007/s12665-021-10026-9

ORIGINAL ARTICLE

Soil–landscape relationship in a sandstone-gneiss topolithosequence in the State of Amazonas, Brazil

Julimar da Silva Fonseca[1] · Milton César Costa Campos[1,2] · Elilson Gomes de Brito Filho[1,2] · Bruno Campos Mantovanelli[3] · Laércio Santos Silva[4] · Alan Ferreira Leite de Lima[1] · José Maurício Da Cunha[1] · Emily Lira Simões[1] · Luís Antônio Coutrim dos Santos[1,5]

Received: 5 July 2020 / Accepted: 30 September 2021 / Published online: 19 October 2021

Abstract

The soil position in the landscape reveals its formation history. Landscapes combine surface features and subsurface components (parent material) of the earth, at which the soil inserts as a three-dimensional and dynamic natural body. The present research aimed to study the soil–landscape relationship in a sandstone-gneiss topolithosequence and the factors determining soil diversification in the State of Amazonas, Brazil. The study extended along a transect of 9253 m, covering the distance between the first and the last profile, for a total of five profiles opened. Profile selection considered landscape topography, from the highest to the lowest relief of the terrain. Soil profiles characterization and classification were based on morphological, chemical, and physical properties and the mineralogy of the clay fraction by X-ray diffraction (XRD). Lithological contrasts and landscape variations determined the different soil types along the topolithosequence. Morphological, physical, chemical, and mineralogical attributes also varied along the landscape. The relief and the parent material, sandstone-gneiss, were the main factors influencing the pedogenesis. Goethite (5–40 g kg^{-1}) was the predominant Fe oxide in all the soils, reflecting the low total iron content ($Fe_t \leq 68$ g kg^{-1}) of the soils and parent materials. The predominance of the sand fraction in all the studied profiles reflected the alluvial nature of the parent material, with the highest values (total sand > 800 g kg^{-1}) occurring in the convex creep slope. Knowing the geomorphic surfaces and the parent material was effective for understanding the variation of the soil attributes along the landscape.

Keywords Amazonian soils · Pedogenesis · Physical attributes · Weathering · Mineralogy

Introduction

The soil is the product of the combinations of factors and formation processes determined by local conditions (Dias et al. 2016). The intensity of these factors and processes promotes progressive transformations in the parent material, which over time are expressed on the morphological, chemical, physical, and mineralogical properties of the soil (Anjos et al. 2007; Miguel et al. 2013; Silva et al. 2020). One of the main factors that influence the diversity and characteristics of Amazonian soils is the rapid weathering of the mineral material by the intense climate of the region, characterized by an extreme water regime and high temperatures (Dalamerlinda et al. 2017). Therefore, identifying the interaction between these factors and their role in soil formation is necessary (Campos et al. 2012a; Silva et al. 2020).

Soil position in the landscape reveals its formation history (Campos et al. 2011; Rodrigues et al. 2016; Capoane et al.

✉ Elilson Gomes de Brito Filho
bfsambiente@gmail.com

[1] Instituto de Educação, Agricultura e Ambiente, Universidade Federal do Amazonas, Humaitá, AM CEP: 69800-000, Brazil

[2] Centro de Ciências Agrárias, Universidade Federal da Paraíba, Areia, PB, Brazil

[3] Agronomy Department, Universidade Federal de Santa Maria, Santa Maria, RS, Brazil

[4] Agronomy Department, Universidade Federal de Rondonópolis, Rondonópolis, Mato Grosso, Brazil

[5] Universidade do Estado do Amazonas, Itacoatiara, AM, Brazil

2017). Thus, the landscape reflects the soil underneath it, which, in turn, determines landscape features and patterns (Minasny and Mcbratney 2006). In general, the soil inherits the characteristics of its parent material. Nevertheless, soil attributes might variate within a local scale as a reflection of rock diversity (Silva et al. 2020) and differences along the toposequence. These determine the specific soil formation processes that occur, and consequently, soil development (Campos et al. 2012a; Braga et al. 2019; Tunçay et al. 2020). Finally, the relief also acts directly on the factors that influence soil characteristics, such as water dynamics and pedogenic processes, and is, therefore, determinant for the variability of soil attributes (Bockheim et al. 2005; Vasconcelos et al. 2012; Li et al. 2015).

To better understand soil distribution in the landscape, a good comprehension of the concepts behind the soil–landscape relationship is crucial for the interpretation of the spatiotemporal variability of soil attributes and the visualization of dynamic processes such as the transport of water, solutes, and sediments (Sommer 2006; Campos et al. 2011). Despite the marked representation of the Middle Madeira River, the predominant physiographic environments are floodplains, native fields, and transition areas, dominated by *Cambissolos*, *Argissolos*, and Entisols. These variations might have a local scale, since in this exuberant landscape, different parent materials originate variations in soil classes and their respective mineralogical, morphological, chemical, and physical properties (Campos et al. 2012a; b).

Several authors have studied the direct effect of the parent material composition on soil formation. Montanari et al. (2010) verified higher contents of goethite and kaolinite in a concave landform compared to linear and convex landforms. On the other hand, the authors also confirmed higher hematite contents in linear landforms. In a toposequence of Oxisols, Curi and Franzmeier (1984) found higher gibbsite concentration in the higher landscape positions. In the lower landscape positions, the authors reported the predominance of kaolinite associated with goethite of low mean crystal diameter. These results reinforce the importance of characterizing soil mineralogy to comprehend the relationship between landscape and parent material. The latter is especially valid for Fe and Al oxides, influenced by the environmental conditions and characterized by their long-term persistence in the soil (Kämpf and Curi 2000).

The diffusion of geotechnologies to elaborate pedological maps in semi-detailed or detailed scales (Lacerda and Barbosa 2012) using soil distribution models that consider the triple interaction between landscape, soil, and parent material (Campos et al. 2007) represents an alternative to be applied. However, implementing these techniques in the Amazon is a big challenge given the territorial extension of the region. Nevertheless, previous studies indicate various characteristics and peculiarities of the Amazonian landscape and have revealed new directions for research regarding the soil–landscape relationship.

It is, therefore, essential to know the soil within the soil–landscape context, to better define its use suitability and limitations (Pedron et al. 2004; Carvalho Filho et al. 2010; Silva et al. 2020). This information can contribute to the strategic planning of land use, mitigating the risks of environmental impacts, especially within the State of Amazonas, which is globally significant. The present research aimed to study the soil–landscape relationship in a sandstone-gneiss topolithosequence and the factors determining soil diversification in the State of Amazonas, Brazil.

Materials and methods

Characterization of the physical environment

The study area is located 150 km from the beginning of the Transamazonic Highway, municipality of Manicoré, State of Amazonas (08°08′12.6″ S and 61°50′06.5″ W). It belongs to the hydrographic basin of Amazonas (Fig. 1). The collection of soil samples occurred between April and May, during the autumn, which is regionally known as the Amazonian winter. According to the Köppen classification (Alvares et al. 2013), the regional climate is Am or rainy tropical (monsoon rains) and has a short dry period. The temperature varies from 25 to 27 °C, and the average annual precipitation is 2.500 mm. The rainy season begins in October and extends until June, with the relative air humidity ranging between 85 and 90%.

The relief characterizes by the presence of plateaus in the highest parts. These have flat topographic surfaces and borders marked by aligned hills and ridges. On the other hand, pediplains occupy the lower areas (CPRM 2001). Regarding the geology, the study area extends over Rondonian Granites characterized by the presence of muscovite, biotite, adamellites, and granodiorites of intrusive cratogenic origin, in the form of stocks and batholiths (Brasil 1978; Melo et al. 2018). According to the ZEE (2008) and Campos et al. (2011), the regional soils are Oxisols. The vegetation in the region is dense, dominated by medium and large trees with a height of up to 50 m (Fig. 2).

The study extended along a transect of 9253 m, from the top of the relief towards the deposition foothill. Measurements of the altitudes were carried out along this transect to make the altimetric profile. Hillside segments were identified based on the model of Dalrymple et al. (1968) using the variation of the terrain slope (Fig. 3).

Five profiles were selected and opened, considering topographic and vegetation variations along the toposequence (Fig. 3). Soil characterization was as follows: P1 = top (08°08′46.0″ S and 61°49′25.1″ W); P2 = colluvial footslope

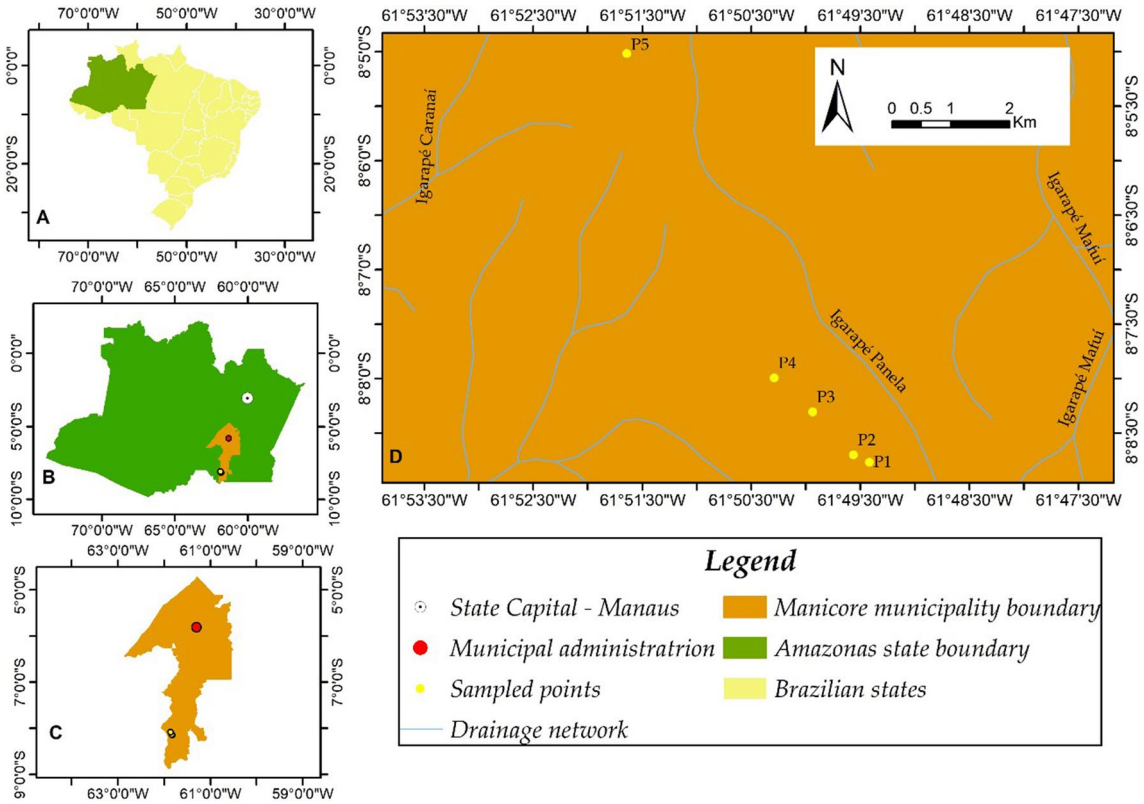

Fig. 1 Location of the profiles studied in the municipality of Manicoré in the state of Amazonas, Brazil

Fig. 2 Images of the collection environment. **A**–Savanna vegetation; **B**–Forest vegetation; **C**–Cerrado vegetation

(08°08′41.8″ S and 61°49′33.9″ W); P3 = convex creep slope (08°08′18.3″ S and 61°49′56.3″ W); P4 = transport foothill (08°07′59.6″ S and 61°50′17.4″ W); and P5 = deposition foothill (08°07′59.6″ S and 61°50′17.4″ W). The identification, morphological description, and sampling of the horizons within the soil profiles followed the methodology proposed by Santos et al. (2018). Soil classification followed the criteria established by the Brazilian Soil Classification System (Santos et al. 2018), the World Reference Base of Soils (IUSS Working Group WRB 2015), and Soil Taxonomy (2014).

Particle size analysis

The pipette method was used to determine particle size in soil samples through chemical and mechanical dispersion with a 0.1 mol L^{-1} NaOH solution and low rotation mechanical stirring for 16 h, respectively (Donagema et al. 2017). The clay fraction was separated by gravitational sedimentation, the coarse and fine sand fraction by sieving, and the silt fraction was calculated by difference.

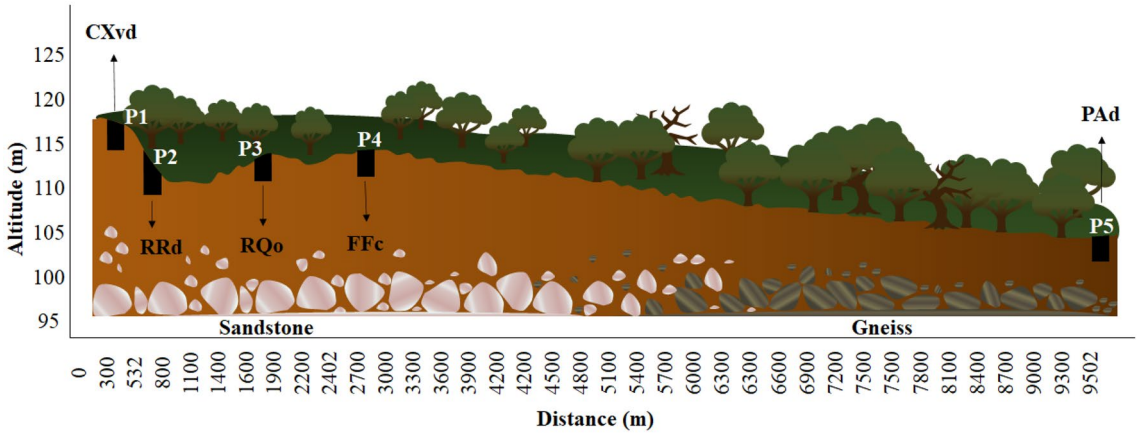

Fig. 3 Schematic profile of the terrain topography and soils in the sandstone-gneiss topolithosequence in the Amazonas state, Brazil. Cambissolo Háplico (CXvd), Neossolo Regolítico (RRd), Neossolo Quartzarênico (RQo), Plintosolo Pétrico (FFc) and Agissolo Amarelo (PAd) in the Amazonas state, Brazil

Chemical analyses

The total iron content (Fe_t) of the clay fraction was determined by selectively dissolving the soil in sulfuric acid (H_2SO_4) in a 1:1 ratio. The latter is a classic procedure in the taxonomy of Brazilian soils in which tropical climate conditions induce Fe concentration in the clay fraction (Donagema et al. 2011). Crystalline free iron (Fe_d) was extracted with sodium dithionite–citrate–bicarbonate (DCB) at 25 °C for 16 h and determined according to Mehra and Jackson (1960). Finally, poorly crystalline iron oxides (Feo) were extracted with ammonium oxalic acid and quantified according to the methodology proposed by McKeague and Day (1966).

Soil pH was determined in water and KCl (1.0 mol L^{-1}), the latter with a KCl to soil solution ratio of 1:2.5 (Donagema et al. 2017). The exchangeable cations Ca^{2+}, Mg^{2+}, and Al^{3+} were extracted with 1.0 mol L^{-1} KCl and measured by atomic absorption spectroscopy. The hydrogen ion and Al^{3+} were extracted with 0.5 mol L^{-1} calcium acetate at pH 7.0 and determined by titration (0.025 mol L^{-1} NaOH) (Donagema et al. 2017). Organic carbon was determined through the wet oxidation method (Walkley and Black, 1934).

The anion exchange resin (AER) was used to extract and quantify bioavailable particulate phosphorus (Pbp). The principle of the AER is the continuous P removal from the solution through exchange with bicarbonate from the resin, creating a concentration gradient that forces P release from the surface of the colloids until an electrochemical equilibrium between the soil and the AER is reached (Skogley and Dobermann 1996).

Bioavailable particulate P extraction followed the methodology developed by Kroth (1998). For this, 0.5 g of soil (1 mm) was added in 15 mL falcon tubes containing 10 mL of distilled water and a sheet of AER saturated with 0.5 mol L^{-1} $NaHCO_3$. These tubes were stirred for 16 h on an end-over-end stirrer (33 rpm) followed by the sheet removal and washing in distilled water and subsequent dilution in 10 mL of 0.5 mol L^{-1} HCl. The tubes remained uncapped for 90 min and then closed and stirred again for 30 min in a horizontal stirrer. Subsequently, a 3 mL aliquot was taken from the extract to determine P content (Murphy and Riley 1962). The sum of bases (SB), the cation exchange capacity (CEC), and base (V) and aluminum (m) saturation were calculated based on the results of the chemical analyses.

Clay mineralogical analysis

The powder X-ray diffraction method served to characterize the minerals of the clay fraction: hematite (Hm), goethite (Gt), kaolinite (Kt), and gibbsite (Gb). The latter required concentrating the iron oxides by boiling the clay fraction in NaOH (Norrish and Taylor 1961) followed by derrification (Mehra and Jackson 1960). Sample diffraction had a scanning speed of 1° 2θ min^{-1} using a Mini-Flex Rigaku II (20 mA, 30 kV) equipped with Cu Kα radiation. The Hm/(Gt + Hm) ratio was estimated by comparing the Hm/(Gt + Hm) peak areas with the proportions obtained from the standard Gt–Hm mixtures. The percentage of Hm and Gt in the clay fraction was expressed as the difference between free (Fed) and poorly crystalline iron (Feo).

The peak areas of Gb (002) and Kt (001) reflections were used to calculate the Kt/(Kt + Gb) ratio. The calculus of the content of isomorphic substitution of iron by aluminum in Gt used the equation mol mol^{-1} = 1730–572 c (Schulze 1984). The content of isomorphic substitution of iron by aluminum in Hm was calculated through the equation mol mol^{-1} = 3098.8–615.12 a0 (Schwertmann et al. 1989).

The specific surface area (SSA) of Gt was estimated by the formula SSA (Gt) = (1049/MCD_{100}^{-5})) (m^2 g^{-1}) (Schulze and Schwertmann 1984), $MCD_{100} = MCD_{110} \times 0.42$ nm (Kämpf 1981), and the SSA of Hm was estimated by the formula SSA (Hm) = 2 × (r + h) × d (m^2 g^{-1}) (Schwertmann and Kämpf 1985). The mean crystal diameter (MCD) of Hm and Gt was calculated from the width at half-height (WHH) and the position of mineral reflections using the Scherrer equation (Klug and Alexander 1974).

Results

Soil distribution in the landscape

The area had a predominately plain physiognomy with minimal relief variations, as typical of Amazonian environments where a gradual field to forest transition occurs. The lowest position of the terrain characterizes by seasonal flooding, and the dominant vegetation consists of small shrub species. Dalrymple et al. (1968) established hypothetical hillside units, which may be partially absent or repeated. In this study, five hillside segments were identified and mapped as a representative toposequence of the region (Fig. 3).

The first three landscape segments–top, colluvial footslope, and convex creep slope–are close to each other and range from 120 to 125 m of elevation. According to Silva et al. (2020), the steep slope of the landscape favors the movement and transport of sediments and water, conditioning the instability of soil attributes and, therefore, originating different soil classes within the same area. The transport foothill represents the third segment. It has 119 m of altitude and might have formed by relief microvariations of the previous section. Its residual erosional character extends from the edges of the lower third until the fifth segment. The fifth segment or deposition foothill varies from 114 to 116 m of altitude, has different topographic characteristics, and can be considered a stable geomorphic environment.

The identification of five different soil classes along the studied segments of the landscape indicates the presence of more than one parent material during pedogenesis. The diverse sandstone-gneiss rocks from which these soils originated suggest the parent material as the principal source of soil attribute differentiation. Knowing the different parent materials in a landscape helps understand the variability of soil attributes, confirming that the geology explains the local relief and the soil patterns (Marques Jr and Lepsch 2000; Campos 2012c).

Morphological and textural attributes

According to the genesis and classification of the soils, all the profiles had a moderate A surface diagnostic horizon (Table 1). Given the topographic position of the top segment (P1), its soil had an incipient B diagnostic subsurface horizon, with no evidence of a predominant pedogenic process. The P1 soil was classified as *CAMBISSOLO HAPLICO Ta Distrófico típico* ((Ochric, Arenic) Dystric Leptic Cambisol).

Soils of the colluvial footslope (P2) and convex creep slope (P3) were poorly evolved, formed by mineral or organic material, with less than 20 cm of thickness, and lacking a diagnostic B horizon. In the P2 segment, the soil was classified as *NEOSSOLO REGOLÍTICO* ((Ochric, Arenic, Dystric) Cambic, Lithic, Leptosol), given its lytic contact (depth > 50 cm) and the occurrence of an A horizon over a C or Cr horizon. The soil of the P2 segment had altered primary minerals, with gravels derived from the ACr horizon (12–35 cm) and the presence of semi-weathered rock fragments (Santos et al. 2013). In the P3 segment, the soil was classified as *NEOSSOLO QUARTZ-RÊNICO* ((Ochric, Arenic) Dystric Regosol) with no lytic contact within the first 50 cm of depth and an A to C sequence of horizons. The texture was sand to loamy sand in all horizons up to a depth of 150 cm, mainly consisting of quartz with coarse and fine sand fractions of whitish colors (Santos et al. 2018).

Seasonal variations of the water table had a marked influence on the soil of the transport foothill (P4), which, therefore, presented small and contrasting reddish mottles in the subsurface horizons. In association with these mottles, plinthite and petroplinthite were also present in amounts varying from common to abundant, which numerically corresponds to 15–40% of the soil volume. These attributes indicate the occurrence of the pedogenic process of plinthization and represent the diagnostic character of the plinthic horizon, according to the Brazilian Soil Classification System (SiBCS) (Santos et al. 2013). From the attributes and horizons identified, the profile was classified, at the suborder level, as *PLINTOSSOLO PÉTRICO Concrecionário típico* ((Ochric, Dystric, Loamy) Petric, Plinthosol).

Finally, the soil profile opened in the deposition foothill (P5) was classified as *ARGISSOLO AMARELO Distrófico abrúptico* (Ochric, Hyperdystric, Clayic) Chromic, Abruptic, Acrisol), presenting a textural B horizon dominated by colors with hues 10 YR and 7.5 YR in the first 100 cm. In this soil, the slope was determinant for the selective removal of clay, contributing to the formation of a textural gradient. In summary, the mineralogical, physical, and chemical attributes of the soils along the topolithosequence accurately elucidated the characteristics of the sandstone-gneiss rocks from which they originated.

Table 1 Morphological and granulometric attributes of a sandstone-gneiss topolithosequence in the Amazonas state, Brazil

Horizon	Depth	Color	Texture	Structure	Clay	Silt	Fine sand	Coarse sand	Total sand	S/C
Top–[1]Cambissolo Háplico Ta Distrófico léptico–CXvd/[2](Ochric, Arenic) Dystric Leptic Cambisol/[3]Inceptisol										
A	0–16	10 YR 3/2	Sandy loam	weak, small, granular	128	182	386	304	690	1.43
AB	16–30	10 YR 3/2	Sandy loam	moderate to medium, angular and subangular blocks	132	198	393	277	670	1.50
Bi	30–55	10 YR 4/6	Sandy loam	weak, medium, angular and subangular blocks	139	213	416	232	648	1.53
BCr	55–78 +	10 YR 4/4	Sandy loam	weak, small to medium, granular, massive structure	142	212	422	224	646	1.49
Coluvial footslope–[1]Neossolo Regolítico Distrofico leptico—RRd / [2](Ochric, Arenic, Dystric) Cambic, Lithic, Leptosol / [3]Entisol										
A	0–12	10 YR 3/2	Sandy loam	weak, small, granular	118	141	241	500	741	1.19
ACr	12–35	10 YR 4/6	Sandy loam	weak, small, angular and subangular blocks, massive structure	111	159	269	460	730	1.43
Cr/Bi	35–62	10 YR 6/6	Sandy loam	weak, small, angular and subangular blocks	116	161	289	441	723	1.33
Convex creep slope–[1]Neossolo Quartzrênico Ortico típico–RQo / [2](Ochric, Arenic) Dystric Regosol / [3]Entisol										
A	0–15	10 YR 3/2	Sand	weak, small to medium, granular	56	53	62	829	891	0.94
C_1	15–33	10 YR 7/2	Sandy loam	weak, large, angular and subangular blocks	50	61	121	768	889	1.21
C_2	33–50	10 YR 7/3	Loamy sand	moderate, medium to large, angular and subangular blocks	49	87	130	734	864	1.78
C_3	50–75	10 YR 7/3	Loamy sand	moderate, medium to large, angular and subangular blocks	59	88	83	770	853	1.49
Cr	75–105 +	10 YR 6/4	Loamy sand	moderate, medium to large, angular and subangular blocks, massive structure	53	98	126	723	849	1.86
Transport foothill–[1]Plintossolo Pétrico concrecionário típico–FFc / [2](Ochric, Dystric, Loamy) Petric, Plinthosol / [3]Ultisol										
A	0–18	10 YR 2/1	Sandy loam	moderate, medium to large, granular	131	306	413	150	563	2.32
AB	18–33	10 YR 3/2	Sandy loam	weak, medium to large, angular and subangular blocks	146	329	467	58	525	2.26
BAf	33–48	10 YR 4/6	Loam	weak to moderate, small to medium, angular and subangular blocks	205	336	435	24	459	1.64
Bf	48–70	10 YR 5/6	Loam	strong, large, angular and subangular blocks	257	360	362	21	383	1.41
BCr	70–110 +	10 YR 6/4	Loam	strong, medium to large, angular and subangular blocks, massive structure	258	297	432	13	445	1.15
Deposition foothill–[1]Argissolo Amarelo Distrofico abruptico–PAd / [2](Ochric, Hyperdystric, Clayic) Chromic, Abruptic, Acrisol / [3]Ultisol										
A1	0–18	10 YR 5/6	Sandy loam	weak, small to large, granular	99	146	406	349	755	1.49
A2	18–32	10 YR 5/6	Sandy loam	moderate, medium to large, angular and subangular blocks	99	172	415	314	729	1.73
AB	32–49	10 YR 5/6	Sandy loam	strong, medium to large, angular and subangular blocks	95	205	416	284	700	2.15
Bt_1	49–74	10 YR 6/8	Clay	strong, medium to large, angular and subangular blocks	548	218	188	47	234	0.40
Bt_2	74–110	10 YR 6/4	Clay	strong, large to very large, angular and subangular blocks	558	228	189	26	215	0.41
Btf	110–125	10 YR 6/8	Clay	strong, large to very large, angular and subangular blocks	563	230	202	5	207	0.41

[1]Brazilian Soil Classification System (Santos et al. 2018)

[2]World Reference Base of Soils (IUSS Working Group WRB, 2015)

[3]Soil Taxonomy (Soil Survey Staff 2014)

S/C silt-to-clay ratio

Soil color in the surface horizons ranged from very dark grayish brown to dark brown (Table 1). However, subsurface horizons had a marked differentiation, varying from yellowish-brown to very pale brown. The grayish tones of most horizons are due to the low concentration of iron oxides and the predominance in the sand fraction of light-colored minerals, such as kaolinite and quartz (Santos et al. 2018). The results confirm this pattern and the predominance of goethite in all the soils, including the Plinthosol with higher hematite contents (Table 3).

Considering the A horizon, the structure of the P1 and P2 profiles was weak, small, granular, with a sandy texture conditioned by the sandstone, which, in turn, obstructs particle bonding (Santos et al. 2018). On the other hand, the gneiss-derived soils had a higher structural variation, with the P3 classified as weak, small to medium, granular, the P4 as a moderate, medium to large, granular, and the P5 as weak, small to large, granular. The increased variability of the A horizon in the P3, P4, and P5 soils revealed strong landscape influence with a low subsurface structural variation. A possible explanation relies on the dynamism or sediment transport and movement in the convex creep slope, transport foothill, and deposition foothill. The steep slope of the landscape contributes to differentiate soil structure, especially in the superficial horizons (Bernini et al. 2013).

According to Silva et al. (2001), the topographic position conditions soil drainage and is, therefore, strongly related to the type of structure. Moderately to well-drained soils tend to have granular or angular and subangular blocky structures, while poorly to imperfectly drained soils generally exhibit a standard structure in polygonal prisms. Relief conditions also influence several soil attributes since the slope creates complex transport patterns of water and solutes, which act on soil profile development (Campos et al. 2012a).

Except for the *Neossolos*, which had a sandy constitution, all profiles had surface horizons with a sandy loam texture (Table 1). The sandstone parent material from the *Palmeiral* Formation and the *Nova Campo Verde* Complex explains the dominance of the sand fraction in these soils. However, attention should be given to the increased clay content in the *Argissolo* within the Bt1–Bt2–Btf horizon. As verified by Campos et al. (2011) and confirmed in the present study, the *Argissolo* and the *Plintossolo*, given their position in the landscape, might have undergone a rejuvenation process, with probable clay loss from their surface horizons and consequent abrupt textural change.

Along the toposequence, morphological differences between the soil profiles indicated the effect of diverse pedogenic factors and processes and confirmed the soil–landscape relationship. According to Ribeiro et al. (2012), the constitution and formation conditions of the soil determine its morphology. Therefore, soil morphology represents a good indicator of previous pedogenic processes and environmental conditions and allows inferring and interpreting soil and plant responses to management practices.

Regarding particle size composition, sand predominated over the other fractions, ranging from 207 to 891 g kg^{-1} (Table 1). The high quartz contents of the parent material (sandstone) might explain these results. High total sand contents were also reported by Schiavo et al. (2010), who characterized and classified soils developed from sandstones of the *Aquidauana* Formation.

Silt contents in the A horizon ranged from 53 to 306 g kg^{-1}, increasing with soil depth (Table 1). Young soils, which are still undergoing formation processes, tend to have low silt contents. Since the studied soils formed from alluvial sediments, particle selection may have occurred, which, in turn, explains the presence of lithogenic (more resistant to changes) and pedogenic materials (with a higher degree of crystallinity). Different from the sand fraction, the clay fraction increased gradually with soil depth and ranged from 48 to 558 g kg^{-1}. Nevertheless, the latter cannot be attributed to the occurrence of the pedogenic process of eluviation and illuviation and might be more likely given by selective removal from surface horizons (sandier), with clay accumulation in the subsurface.

The *Neossolos* presented higher proportions of coarse fractions (> 2 mm) with consolidated ferruginous material (plinthite and petroplinthite). Decreased levels of the water table might have enhanced the drainage, as suggested by the presence, within the first 48 cm of the soil, of a more reddish hue (2.5 YR) than in the other profiles (Table 1). The predominance of coarse sand fractions combined with the remarkable presence of gravels indicates that the weathering processes in this soil did not promote a significant fragmentation of these fractions (Lima et al. 2008).

In the transport foothill (P4), clay contents ranged from 95 to 99 g kg^{-1} in the A, AB, and BA horizons, reaching values of up to 548 g kg^{-1}, 558 g kg^{-1}, and 567 g kg^{-1} in the Bt1, Bt2, and Btf horizons, respectively. The marked textural differentiation between the A and Bt1 horizons characterizes an abrupt textural change with a significant increase of clay compared to the overlying horizons (Table 1).

At the top (P1), colluvial footslope (P2) and convex creep slope (P3), the silt-to-clay ratio (S/C) ranged from 1.43–1.50, 1.19–1.43, and 0.94–1.86, respectively (Table 1), associated with the lower development of these soils. The transport foothill (P4) had the lowest S/C ratio, with values between 0.7 and 0.8. On the contrary, the deposition foothill presented the highest ratios, ranging from 1.49 in the surface horizons to 0.41 in the deeper ones. According to Campos et al. (2011), higher S/C values are due to clay loss or slight increases in the silt fraction, suggesting that minor relief variations provide relative losses

or gains and, probably not given by changes in the parent material.

Clay and silt contents tended to increase towards the youngest geomorphic surfaces, this is, from the top (P1) towards the transport (P4) and deposition foothills (P5). The opposite direction of this pattern compared to that of the total sand reflects the recent sedimentary nature of these fractions, since the soils of these geomorphic environments are closely related to the parent material. Similar results were reported by Campos et al. (2012b) when studying the soil-geomorphic surface relationships of a floodplain-upland toposequence in the region of Humaitá, Amazonas, Brazil.

Variations of chemical attributes

The values of pH ranged from 4.17 to 5.48 (H_2O) and 3.81 to 5.70 (KCl), especially in the top (P1) and deposition foothill (P5), presenting the highest acidity content in the surface horizon. According to Campos et al. (2012b), the high regional precipitation contributes significantly to base leaching, increasing soil pH. The balance of negative net charges,

Table 2 Soil chemical attributes in a sandstone-gneiss topolithosequence in the Amazonas state, Brazil

Horizon	pH		Ca^{2++}	Mg^2	K^+	SB	Al^{3+}	H + Al	CEC	m	V	P resina	OC
	H_2O	KCl	$cmol_c\ dm^{-3}$							%		$mg\ dm^{-3}$	$g\ kg^{-1}$
Top–[1]Cambissolo Háplico Ta Distrófico léptico–CXvd / [2](Ochric, Arenic) Dystric Leptic Cambisol / [3]Inceptisol													
A	4.79	3.81	1.00	0.15	0.12	1.27	4.3	19.42	21	77	6	4.6	5.93
AB	4.94	4.50	0.20	0.14	0.11	0.35	4.4	19.38	20	93	2	3.1	2.65
Bi	4.62	4.42	0.30	0.09	0.12	0.51	4.9	18.48	19	91	3	2.8	3.14
BCr	5.11	4.34	0.20	0.06	0.07	0.33	4.8	19.32	20	94	2	2.4	1.59
Coluvial footslope–[1]Neossolo Regolítico Distrofico leptico–RRd / [2](Ochric, Arenic, Dystric) Cambic, Lithic, Leptosol / [3]Entisol													
A	4.17	3.89	0.40	0.17	0.11	0.68	5.5	18.21	19	87	4	3.9	4.74
ACr	4.94	4.30	0.20	0.14	0.09	0.43	5.4	16.23	17	91	3	2.7	3.03
Cr/Bi	5.19	4.25	0.30	0.14	0.09	0.53	5.2	14.47	15	89	4	2.8	2.63
Convex creep slope–[1]Neossolo Quartzrênico Ortico típico–RQo / [2](Ochric, Arenic) Dystric Regosol / [3]Entisol													
A	4.91	4.16	0.20	0.12	0.09	0.41	4.3	19.17	20	91	2	2.6	4.81
C_1	5.2	4.70	0.40	0.12	0.06	0.58	5.3	17.25	18	90	3	2.0	3.46
C_2	4.97	4.43	0.40	0.12	0.08	0.60	5.5	15.88	16	90	4	2.1	1.97
C_3	4.72	4.16	0.20	0.12	0.08	0.40	5.7	17.77	18	93	2	2.2	0.63
Cr	4.8	4.13	0.50	0.15	0.10	0.75	5.6	18.21	19	88	4	2.1	0.01
Transport foothill–[1]Plintossolo Pétrico concrecionário típico–FFc / [2](Ochric, Dystric, Loamy) Petric, Plinthosol / [3]Ultisol													
A	4.95	3.97	0.40	0.17	0.12	0.69	3.9	26.03	27	85	3	3.1	5.10
AB	5.03	4.19	0.20	0.06	0.09	0.34	3.9	23.73	24	92	1	1.9	4.24
BAf	5.20	4.17	0.60	0.17	0.11	0.88	3.1	18.86	20	78	4	1.4	3.76
Bf	5.35	4.42	0.20	0.09	0.06	0.35	3.5	19.43	20	91	2	1.7	3.26
BCr	5.48	4.52	0.30	0.12	0.06	0.48	3.5	18.15	19	88	3	0.7	2.91
Deposition foothill–[1]Argissolo Amarelo Distrofico abruptico–PAd / [2](Ochric, Hyperdystric, Clayic) Chromic, Abruptic, Acrisol / [3]Ultisol													
A1	4.23	3.88	0.30	0.15	0.13	0.58	4.3	27.72	28	88	2	5.8	6.98
A2	4.33	4.06	0.70	0.12	0.10	0.92	4.3	24.98	26	82	4	3.3	4.33
AB	4.74	4.15	0.20	0.06	0.06	0.32	4.9	18.66	19	94	2	2.0	3.72
Bt_1	4.83	4.22	0.70	0.09	0.07	0.86	4.2	26.5	27	83	3	2.1	3.16
Bt_2	4.8	4.25	0.60	0.17	0.06	0.84	4.6	25.86	27	85	3	2.2	3.14
Btf	4.23	3.88	0.30	0.15	0.13	0.84	4.9	24.73	26	85	3	2.1	1.06

[1]Brazilian Soil Classification System (Santos et al. 2018)

[2]World Reference Base of Soils (IUSS Working Group WRB 2015)

[3]Soil Taxonomy (Soil Survey Staff 2014)

SB sum of bases; *CEC* cation exchange capacity; *V* base saturation; m: aluminum saturation; *OC* organic carbon

expressed by ΔpH in the B horizon, showed the highest values at the top (P1), which corresponds with the trend of poorly evolved soils in the youngest surface (Table 2).

The bases Ca^{2+}, Mg^{2+}, and K^{+} ranged from 0.20 to 1.0 $cmol_c\ kg^{-1}$ (Table 2). In general, these elements had only slight variations along the toposequence, given their reduced levels in the minerals of sandstone-gneiss and the regional climate conditions, which favor advanced soil weathering. Moreover, the predominance of oxidic minerals generated positive charges, which, allied with the sandier texture, provided the movement or loss of these cations to subsurface horizons. This pattern, however, does not apply to K, which remained at higher concentrations near the soil surface. According to Neves et al. (1961) and Prietzel et al. (2020), this is a characteristic attributed to the low diffusion power electrostatically adsorbed to negative charges of organic matter or the formation of sphere complexes external to the solid phase.

Exchangeable aluminum (Al^{3+}) content had no significant variation along the topolithosequence, with low values recorded in all profiles, mainly in the A horizon. In addition, the potential acidity (H^{+} and Al^{3+}) values were high and increased in depth along the topolithosequence (Table 2). Possibly, the intense rainy season of the region and the unimpeded drainage were determining climate factors for edaphic acidity as soil depth increased (Campos et al. 2012).

Along the topolithosequence, organic carbon (OC) contents were higher in the surface horizons because of the concentration of organic matter from the decomposition of native vegetation residues (Santos et al. 2012). Cation exchange capacity (CEC) ranged from high to very high (12–28 $cmol_c\ dm^{-3}$). The same trend occurred for the sum of bases (SB), which was higher in the A horizon because of the levels of OC and the low clay content and activity.

Due to the low activity of the clay fraction, all segments were classified as dystrophic (Table 2), which is the result of base depletion (Ca^{2+}, Mg^{2+}, and K^{+}). Other authors have reported similar results in the Amazonian region (Campos et al. 2012a; Santos et al. 2012; Martins et al. 2006). The geomorphic surface, that is, the landscape did not influence the variation of the SB. It is, therefore, inferred that the soil inherited the chemical poverty from the gneiss and sandstone rocks, revealing the parent material as the determinant formation factor for the dystrophic character of the soils along the topolithosequence. These results differ from those reported by Campos et al. (2010), who verified a higher degree of soil development and dominance of dystrophic soils at the top positions of the landscape.

Soils along the topolithosequence were Álico, with aluminum saturation (m) ranging from 51 to 91%. These values resemble those reported by Martins et al. (2006) for soils in a field to forest transition in the region of Humaitá, Amazonas, Brazil. This is an inherent characteristic of the sandstone-gneiss, which has by nature an acidic character. As mentioned, the Al^{3+} richness justifies the formation of gibbsite in the *Neossolos* (P2 and P3).

Available phosphorus (P) contents did not vary along the topolithosequence and were on average 2.0 mg kg^{-1}, decreasing with soil depth. According to Silva et al. (2006), P in the deeper horizons remains stable due to its low mobility. The strong affinity of iron oxides, especially goethite, with P also promotes its retention (Pinto et al. 2013; Rotta et al. 2015). The high isomorphic substitution (IS) and SSA of Gt in goethite-rich soils, like those in the present study, also potentialize P adsorption. However, available P in the A horizon of the top (P1), transport (P4), and deposition (P5) foothills were 4.6, 3.1, and 5.8 mg kg^{-1}, respectively, representing the highest values in the topolithosequence. The latter could be associated with the accumulation of OC as litter on the soil surface horizon. The OC acts as a physical barrier, inhibiting the direct contact of P with the active

Table 3 Crystallographic attributes of soil minerals of a sandstone-gneiss topolithosequence in the Amazonas state, Brazil

Soil	Content					Ratio			MCD				WHH		SSA		IS	
	g kg^{-1}								°2θ						$m^2\ g^{-1}$		mol mol^{-1}	
	Fe_t	Fe_o	Fe_d	Gt	Hm	Kt/(Kt + Gb)	Fe_o/Fe_d	Fe_d/Fe_t	Gt_{110}	Gt_{111}	Hm_{110}	Hm_{012}	Kt	Gb	Gt	Hm	Gt	Hm
CXvd_AB	36	7.4	17	24	5	0.56	0.44	0.47	20.6	9.4	21.6	31.1	0.5	0.25	116.3	54.4	0.43	0.07
CXvd_Bi	28	5.6	12	21	5	0.45	0.47	0.43	15.2	8.9	16.4	54.6	0.51	0.31	159.7	79.9	0.15	0.02
RRd_ACr	12	3.1	5	5	1	0.87	0.62	0.42	25.1	18.2	25.4	28.3	0.5	0.17	94.6	41.3	0.38	0.04
RQo_Cr	9	1.8	3	5	1	0.76	0.60	0.33	25.1	13.9	12.8	36.6	0.7	0.28	94.6	89.4	0.33	0.02
FFc_Bf	35	4.2	21	41	9	0.37	0.20	0.60	18.5	14.9	22.8	30.2	ni	0.34	130.1	47.2	0.39	0.12
FFc_BAf	41	4.9	25	40	9	0.41	0.20	0.61	10.4	7.8	15	89.6	0.48	0.3	234.3	78.6	0.31	0.11
PAd_Bf	68	8.2	52	39	9	0.63	0.16	0.76	23.7	11.9	13.9	63	0.55	0.28	100.5	77.5	0.36	0.17
PAd_Btf	64	7.7	41	25	5	0.60	0.19	0.64	28.4	21.2	17.7	49.1	0.5	0.27	82.93	63.5	0.44	0.13

Fet total iron; *Feo* poorly crystalline iron; *Fed* crystalline iron; *MCD* mean crystal diameter; *WHH* width at half-height, *SSA* specific surface area, *IS* isomorphic substitution; *Gt* goethite; *Hm* hematite; *Kt* kaolinite; Gb: gibbsite; *ni* not identified

sites, therefore, enabling P occurrence in the available soil fraction (Fink et al. 2014).

Fe content and mineralogical attributes

The contents of total Fe (Fe_t, 9–68 g kg^{-1}), Fe extracted from crystalline oxides (Fe_d, 3–52 g kg^{-1}), and poorly crystalline Fe oxides (Fe_o, 1.8–8.2 g kg^{-1}) were low (Table 3) (Kämpf and Curi 2000). Lima et al. (2006) and Aquino et al. (2016) reported similar results for Amazonian environments. The low Fe_t is typical of the naturally poor levels of Fe minerals in the sandstone and gneiss rocks from which the soils derived and frame these soils as hypoferric ($Fe_t \leq 80$ g kg^{-1}) according to the current taxonomic system of Brazilian soils–SiBCS (Santos et al. 2018). The levels of Fe_d were higher than those of Fe_o, especially in the most weathered soils (PAd) and in those with the presence of plinthite, a Fe-rich clay agglomerate, in the diagnostic B horizon of FF. Although lower than Fed, high Feo contents marked the soils CXvd_AB (7.4 g kg^{-1}), PAd_Btf (7.7 g kg^{-1}), and PAd_Bf (8.2 g kg^{-1}). The sandy texture and high levels of organic matter in the superficial horizons of these soils explain their Feo contents. These characteristics can promote Fe loss, inhibiting the crystallization of Fe oxides, this is, the formation of poorly crystalline compounds (Schwertmann and Taylor 1989; Anjos et al. 2007; Miguel et al. 2013).

The predominance of Fe_d culminated in low Fe_o/Fe_d values (≤ 0.5), mainly for the B horizon of the FF and PAd due to the presence of plinthite. Higher Fe_o/Fe_d values might reflect the occurrence of the poorly crystalline Fe oxide ferrihydrite in the system, mainly in RQo_Cr and CXvd_Bi, indicating water stagnation in the profile of these soils. The crystalline Fe forms (hematite and goethite) found as plinthite or within pretro-plinthite might dissolve, giving place to a new generation of poorly crystalline Fe oxides, such as ferrihydrite, for instance (Coelho and Vidal-Torrado 2003; Miguel et al. 2013).

The Fe_d/Fe_t ratio indicated different degrees of pedogenesis along the topolithosequence (Table 3). In general, the lower the Fe_d/Fe_t ratio, the higher the proportion of Fe released through the weathering of lithogenic minerals for the neoformation of pedogenic Fe oxides such as goethite and hematite, which are the main constituents of tropical soils (Silva et al. 2020). More than 50% of the Fe_t was represented by Fe_d, which associated with the reduction of the Fe_d/Fe_t ratio indicated higher pedogenesis following the sequence PAd_Bf > PAd_Btf > FFc_BAf > FFc_Bf > CXvd_AB > CXvd_Bi > RRd_ACr > RQo_Cr. Increased Fed values are associated with good vertical drainage and a marked chemical transformation in soils favorable to the crystallinity of pedogenic Fe oxides such as goethite and hematite (Kämpf and Curi 2000; Lima et al. 2006; Cornell and Schwertmann 2003; Camelo et al. 2018; Poggere et al. 2018; Silva et al. 2020). Finally, Fe contents, although low, proved to be sensible environmental pedoindicators, as attributed by Silva et al. (2020) when evaluating the influence of the parent material and the cause–effect relationship of landscape dissection on soil genesis and the mineralogical variability of the clay fraction in basalt-sandstone Brazilian environments.

The minerals kaolinite (Kt), gibbsite (Gb), hematite (Hm), and goethite (Gt) were all present in the clay fraction of the diagnostic and transitional B horizons (Table 3). Along the toposequence, the Fe oxides Hm and Gt followed the order: transport foothill (9–41 g kg^{-1}) > deposition foothill (5–39 g kg^{-1}) > top (5–24 g kg^{-1}) > colluvial footslope and convex creep slope (1–5 g kg^{-1}). Among the iron oxides, Gt was present in the clay fraction of all the studied soils, which is given by the iron poverty of the sandstone-gneiss sediments (Correa et al. 2008; Santos et al. 2010; Silva et al. 2020; Brito et al. 2021). This lithological condition might have favored Gt formation (Barrón and Torrent 2002; Silva et al. 2020), as suggested by the low Hm contents, with a maximum value of 9 g kg^{-1} in the topolithosequence.

The crystallographic parameters MCD, WHH, SSA, and IS reflected the peculiarities of the topolithosequence (Table 3). The mean crystal diameter (MCD) in the Gt_{110} and Gt_{111} peaks varied from 10 to 28 nm and 9 to 21 nm, respectively. These values were lower than those detected for the Hm_{111} and Hm_{012} peaks, which were 12–25 nm and 30–89 nm, respectively. Overall, MCD values revealed the persistence of crystalline Hm over Gt, as commonly reported for tropical soils (Inda Jr and Kämpf 2005; Barbieri et al. 2014). The latter was evident in the transport foothill (P4), where Hm_{012} peaks were well-defined and narrow (Fig. 4). The climatic conditions of the Amazonian region, especially precipitation and temperature, combined with the naturally high contents of OM, the acid pH (Table 2), and the intense microbial activity, increase Al presence in the goethite structure and, in turn, decreases its crystallinity. Except for the top segment (P1), the isomorphic substitution (IS) along the topolithosequence surpassed 0.33 mol mol^{-1}, indicating the occurrence of markedly weathered, non-hydromorphic, and acid soils (high Al activity) (Table 2).

These conditions justify the persistence of Gt with high Fe substitution ($r = 0.065$) by Al ($r = 0.053$), which promoted the contraction of the unit cell and, consequently, increased the specific surface area (SSA) that ranged between 82 and 234 m^2 g^{-1} in Gt and 41–89 m^2 g^{-1} in Hm. These results are consistent with previous research in Brazilian soils (Melo et al. 2001; Correa et al. 2008) since the higher IS and SSA values in Gt reflect its higher structural capacity to accommodate Al compared to Hm (Schwertmann and Taylor 1989; Carvalho Filho et al. 2015).

Iron oxides concentrated in the soils of each landscape segment following the order: transport foothill (P4) > deposition foothill (P5) > top (P1) > convex creep slope (P3) and

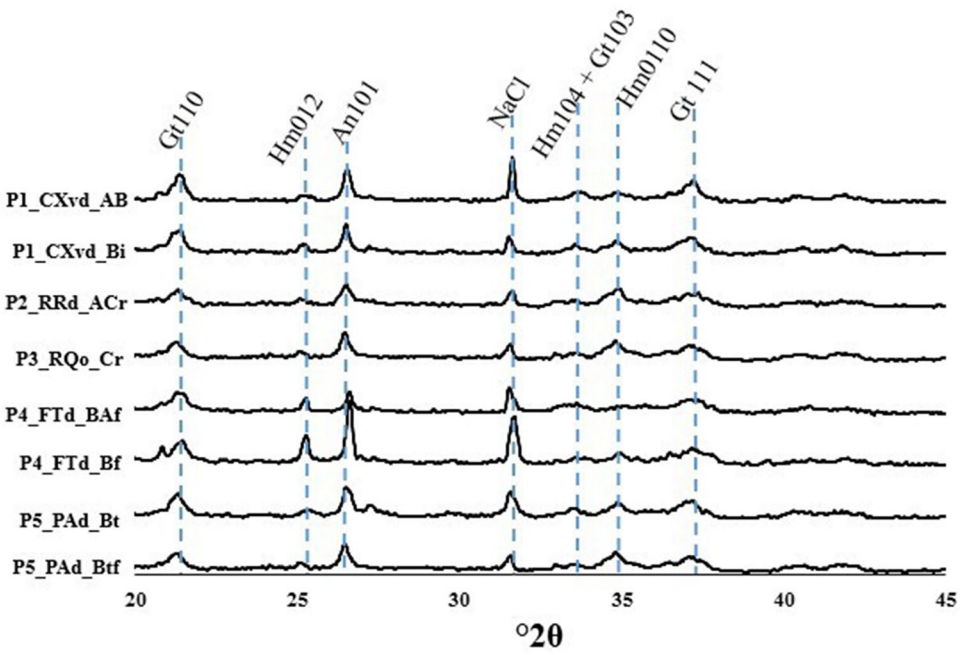

Fig. 4 X-ray diffractograms of the clay fraction for hematite (Hm) and goethite (Gt) in the profiles of Cambissolo Háplico (CXvd-AB; CXvd-Bi), Neossolo Regolítico (RRd-ACr), Neossolo Quartzarênico (RQo-Cr), Plintosolo Pétrico (FFc-Bf; FFc-BAf) and Argissolo Amarelo (PAd-Bt; PAd-Btf) in the Amazonas state, Brazil

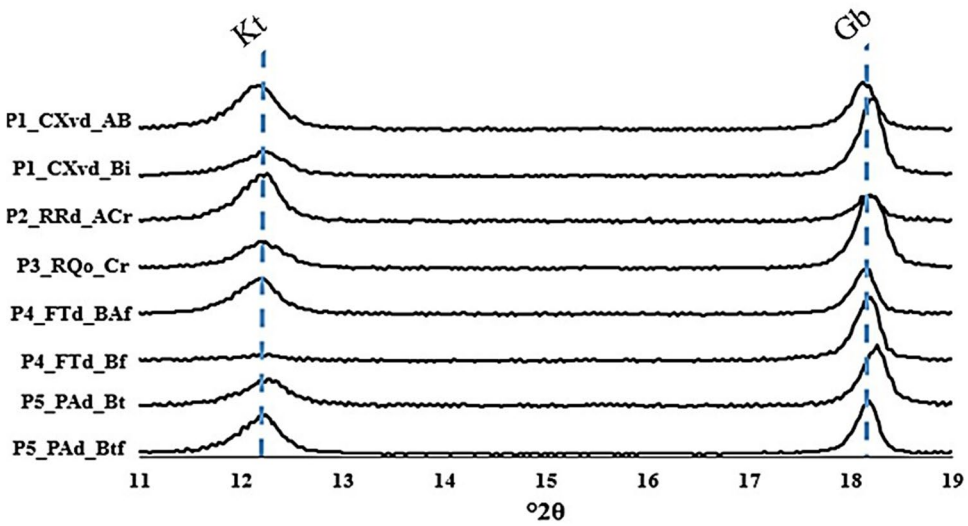

Fig. 5 Pattern of X-ray diffractograms of the clay fraction for kaolinite (Kt) and gibbsite (Gb) in the profiles of Cambissolo Háplico (CXvd-AB; CXvd-Bi), Neossolo Regolítico (RRd-ACr), Neossolo Quartzarênico (RQo-Cr), Plintosolo Pétrico (FFc-Bf; FFc-BAf) and Argissolo Amarelo (PAd-Bt; PAd-Btf) in the Amazonas state, Brazil

colluvial footslope (P2) (Table 3 and Fig. 4). The highest levels of Fe oxides, especially Hm, in the *Plintossolo* (P4), are given by the increased iron contents in the BAf and Bf horizons, characterized by the presence of ferruginous concretions, as typical of Amazonian *Plintossolos* (Campos et al. 2012). Even in poorly developed soils such as the RQo_Cr, marked by the occurrence of lytic contact (weak rock or outcropping saprolite), well-defined peaks of Gt formed (Fig. 4). This fact was already expected since goethite is the first Fe oxide that forms in the initial horizons close to the rock during the early stages of pedogenesis (Curi and Franzmeier 1984; Silva et al. 2020).

The Kt/(Kt + Gb) ratio indicated Gb as an important mineralogical constituent of the studied soils, except for the top and the deposition foothill (P5) (Table 2 and Fig. 5). The low Kt contents or even its absence in the transport foothill (P4) might reflect the disruption of Kt nucleation probably due to increased contents of iron oxides as previously reported by Gidhin et al. (2006). Consequently, Kt had higher width at half-height (WHH) (0.483–0.703 nm) than Gb crystals (0.273–0.307 nm). This result indicates that Gb crystals are much more crystalline than Kt, which is characteristic of highly weathered soils (Ghidin et al. 2006; Camargo et al. 2008), where low Si concentrations favor the formation of Gb crystals in the soil (Hsu 1989).

The proportions of Kt, as expressed by the [Kt/Kt + Gb > 75] ratio, and the low contents of Fe oxides indicate low pedogenic intensity or predominance of morphogenesis over pedogenesis in the *Neossolos* (Scarciglia et al. 2005). Thus, geomorphological characteristics such as the more rugged and dissected topography of the landscape segments characterized by the presence of *Neossolos* (Fig. 3) favored the partial removal of basic cations and silicon, which combine in the soil to form Kt (Kämpf et al. 2009). Additionally, part of the Si and Al removed from the soil through weathering in the top segment of the landscape could have been transported and accumulated in the lower landscape positions, increasing the [Kt/Kt + Gb > 60] ratio in the *Argissolo* (P5). These results are supported by previous research (Curi and Franzmeier 1984; Ghidin et al. 2006; Campos et al. 2007; Silva et al. 2020), which considered the landscape a passive factor of soil formation and retribution of pedogenic minerals.

Final considerations

Differentiating the landscape into segments and identifying the parent material were efficient to understand the variation of soil attributes along the studied transect. Soil classes depend on the topography and the parent material, thus varying with the physical, chemical, morphological, and mineralogical properties. Mineralogically, the clay fraction is composed of kaolinite, goethite, hematite, and gibbsite, with goethite being the predominant iron oxide. Additionally, as confirmed by soil mineralogy, the chemical properties of the cations of exchangeable bases from sediments originated from these soils were naturally poor in bases and, therefore, not related to the removal process of the system, as widely recognized in the Amazonian region.

Independently of the surface, the sand fraction dominated over the other fractions. The alluvial nature of the parent material explains this result, with the highest values occurring in the *Neossolos* and increasing with the depth of the soil profile.

Conclusions

Lithological contrast and landscape variations determined the different soil types as well as morphological, physical, chemical, and mineralogical attributes in the topolithosequence. The relief and the parent material, sandstone-gneiss, were the main factors influencing pedogenesis. Goethite was the predominant Fe oxide in all the soils, reflecting the low total iron content of the parent material. The predominance of the sand fraction in all the studied profiles reflected the alluvial nature of the parent material, with the highest values occurring in the convex creep slope. Knowing the geomorphic surfaces and the parent material was effective for understanding the variation of the soil attributes along the landscape.

Funding Conselho Nacional de Desenvolvimento Científico e Tecnológico (CNPq), Coordenação de Aperfeiçoamento de Pessoal de Nível Superior (CAPES), and Fundação de Amparo à Pesquisa no Estado do Amazonas (FAPEAM).

Data availability The data that support the findings of this study are available from the corresponding author, L.S.S., upon reasonable request.

Code availability Not applicable.

Declarations

Conflict of interest Related to submission and processing within the journal, the authors of that work declare that there is no conflict of interest or similar situation in relation to that work.

Ethical approval This article does not contain any studies with human participants or animals performed by any of the authors.

References

Alvares CA, Stape JL, Sentelhas PC, Gonçalves JLM, Sparovek G (2013) Köppen's climate classification map for Brazil. Meteorol Z 22:711–728. https://doi.org/10.1127/0941-2948/2013/0507

Anjos LHC, Pereira MG, Pérez DV, Ramos DP (2007) Characterization and classification of plintosols from Pinheiro, Maranhão state, Brazil. Rev Bras Ciênc Solo 31:1035–1044. https://doi.org/10.1590/S0100-06832007000500020

Aquino RE, Marques J Jr, Campos MCC, Oliveira IA, Bahia ASRS, Santos LAC (2016) Characteristics of color and iron oxides of clay fraction in archeological dark earth in Apuí region, southern Amazonas. Geoderma 262:35–44. https://doi.org/10.1016/j.geoderma.2015.07.010

Barbieri DM, Marques J Jr, Siqueira DS, Teixeira DB, Panosso AR, Pereira GT, La Scala JN (2014) Iron oxides and quality of organic matter in sugarcane harvesting systems. Rev Bras Ciênc Solo 38:1143–1152. https://doi.org/10.1590/S0100-06832014000400010

Barrón V, Torrent J (2002) Evidence for a simple pathway to maghemite in earth and mars soils. Geochim Cosmochim Acta 66:2801–2806. https://doi.org/10.1016/S0016-7037(02)00876-1

Bernini TA, Pereira MG, Fontana A, Anjos LHC, Calderano SB, Wadt PGS, Moraes AGL, Santos LL (2013) Taxonomy of soils developed under sedimentary deposits from Solimões formation in Acre state, Brazil. Bragantia 72:71–80. https://doi.org/10.1590/S0006-87052013005000014

Bockheim JG, Gennadiyev NA, Hammer RD, Tandarich JP (2005) Historical development of key concepts in pedology. Geoderma 124:23–36. https://doi.org/10.1016/j.geoderma.2004.03.004

Braga LM, Caldeira D, Nunes JGDS, Hussain Y, Carvajal HM, Uagoda R (2019) Caracterização geomorfológica e dinâmica

erosivo-deposicional de encostas no vale fluvial do ribeirão Contagem-DF, Brasil. Anuário Do Instit Geoci 41:51–65
BRASIL (1978) Ministério das Minas e Energia. Projeto Radambrasil, folha SB. 20. Purus, Rio de Janeiro
Brito WB, Campos MC, Souza FG, Silva LS, Cunha JM, Lima AF, Martins TS, Oliveira FP, Oliveira IA (2021) Spatial patterns of magnetic susceptibility optimized by anisotropic correction in different Alisols in southern Amazonas, Brazil. Precision Agric 28:1–31. https://doi.org/10.1007/s11119-021-09843-6
Camargo LA, Marques J Jr, Pereira GT, Horvat R (2008) Spatial variability of mineralogical attributes of an oxisol under different relief forms: I - clay fraction mineralogy. Rev Bras Ciênc Solo 32:2269–2277. https://doi.org/10.1590/S0100-06832008000600006
Camêlo DL, Ker JC, Fontes MPF, Costa ACS, Corrêa MM, Leopold M (2018) Mineralogy, magnetic susceptibility and geochemistry of Fe-rich Oxisols developed from several parent materials. Sci Agric 75:410–419. https://doi.org/10.1590/1678-992x-2017-0087
Campos MCC (2012) Soil-landscape relationships: concepts, developments and applications. Ambiência 8:963–982. https://doi.org/10.5777/ambiencia.2012.05.01rb
Campos MCC, Marques J Jr, Pereira GT, Montanari R, Camargo LA (2007) Soil-landscape relationships in a sandstone-basalt lithosequence in Pereira Barreto, São Paulo. Rev Bras Ciênc Solo 31:519–529. https://doi.org/10.1590/S0100-06832007000300012
Campos MCC, Ribeiro MR, Souza Júnior VS, Ribeiro Filho MR, Costa EUC (2010) Slope segments and soil properties of a toposssenquence in the Manicoré region, AM. Cienc Agron 41:501–510. https://doi.org/10.1590/S1806-66902010000400001
Campos MCC, Ribeiro MR, Souza Júnior VS, Ribeiro Filho MR, Souza RVC (2011) Soil-landscape relationships on a granite substrate toposequence in Santo Antônio do Matupi, Manicoré, Amazonas. Rev Bras Ciênc Solo 35:13–23. https://doi.org/10.1590/S0100-06832011000100002
Campos MCC, Ribeiro MR, Souza Júnior VS, Ribeiro Filho MR, Souza RVCC, Almeida MC (2012) Soil-relief relationships in a grassland/forest transition in the region of Humaitá, Amazonas State, Brazil. Acta Amazon 42:387–398. https://doi.org/10.1590/S0044-59672012000300011
Capoane V, Tiecher T, Santos DR (2017) Variation of soil attribute along of three toposequence in the Rio Grande do Sul plateau. Rev Bras Geogr Fís 10:1435–1454. https://doi.org/10.26848/rbgf.v10.5.p1435-1454
Carvalho Filho A, Inda Júnior AV, Fink JR, Curi N (2015) Iron oxides in soils of different lithological origins in Ferriferous Quadrilateral (Minas Gerais, Brazil). Appl Clay Sci 118:01–75. https://doi.org/10.1016/j.clay.2015.08.037
Coelho MR, Vidal-Torrado P (2003) Caracterização e gênese de perfis plínticos desenvolvidos de arenito do Grupo Bauru: II - mineralogia. Rev Bras Ciênc Solo 27:495–507. https://doi.org/10.1590/S0100-06832003000300011
Cornell RM, Schwertmann U (2003) The iron oxides: structure, properties, reactions, occurrences and uses, 2nd edn. Wiley-VCH Verlag GmbH & Co
Correa MM, Ker JC, Barrón V, Fontes MPF, Torrent J, Curi N (2008) Caracterização de óxidos de ferro de solos do ambiente tabuleiros costeiros. Rev Bras Ciênc Solo 32:1017–1031. https://doi.org/10.1590/S0100-06832008000300011
CPRM (2001) Serviço geológico do Brasil. Geologia e recursos minerais do estado do amazonas. Boletim Técnico. CPRM, Manaus
Curi N, Franzmeier DP (1984) Toposequence of oxisols from the central plateau of Brazil. Soil Sci Soc Am J 48:341–346. https://doi.org/10.2136/sssaj1984.03615995004800020024x
Dalamerlinda EA, Souza Júnior VS, Wadt PGS, Deng Y, Campos MCC, Câmara ERG (2017) Soillandscape relationship in a chronosequence of the middle Madeira River in southwestern Amazon, Brazil. CATENA 149:199–208. https://doi.org/10.1016/j.catena.2016.09.021
Dalrymple JB, Blong RJ, Conacher AJ (1968) An hypothetical nine unit landsurface model. Z Geomorphology 12:60–76
Dias LMDS, Coelho RM, Valladares GS, Assis ACCD, Ferreira EP, Silva RCD (2016) Soil class prediction by data mining in an area of the sedimentary São Francisco basin. Pesqui Agropecu Bras 51:1396–1404. https://doi.org/10.1590/S0100-204X2016000900038
Donagema GK, Campos DVB, Calderano SB, Teixeira WG, Viana JHM (2011) Manual de métodos de análises de solos, 2nd edn. Embrapa Solos
Donagema GK, Campos DVB, Calderano SB, Teixeira WG, Viana JHM (2017) Manual de métodos de análise de solo, 3rd edn. Embrapa Solos
Fink JR, Inda AV, Bayer C, Torrent J, Barrón V (2014) Mineralogy and phosphorus adsorption in soils of south and central-west Brazil under conventional and no-tillage systems. Acta Sci Agron 36:379–387. https://doi.org/10.4025/actasciagron.v36i3.17937
Ghidin AA, Melo VF, Lima VC, Lima JMJC (2006) Oxisol toposequences developed from basaltic rocks in Paraná State, Brazil: I - clay fraction mineralogy. Rev Bras Ciênc Solo 30:293–306. https://doi.org/10.1590/S0100-06832006000200010
Hsu PH (1989) Aluminiun oxides and oxyhydroxides. In: Dixon JB, Weed SB (eds) Minerals in soil environments, 2nd edn. Soil science society of America, pp 331–378
Inda Júnior AV, Kämpf N (2005) Variability of goethite and hematite via reductive dissolution in soils of the tropical and subtropical. Rev Bras Ciênc Solo 29:851–866. https://doi.org/10.1590/S0100-06832005000600003
IUSS Working Group WRB (2015) World reference base for soil resources 2014, update 2015: International soil classification system for naming soils and creating legends for soil maps. FAO, Rome. (World Soil Resources Reports, 106).
Kämpf N (1981) Die Eisenoxidmineralogie einer Klimasequenz von Böden aus Eruptiva in Rio Grande do Sul. Thesis, Technische Universitat München
Kämpf N, Curi N (2000) Tópicos em ciência do solo - óxidos de ferro: Indicadores de ambientes pedogênicos e geoquímicos. Sociedade Brasileira de Ciência do Solo, pp 107–138
Kämpf N, Curi N, Marques J Jr (2000) Óxidos de alumínio, silício, manganês e titânio. In: Melo VF, Alleoni LRF (eds) Química e mineralogia do solo. Sociedade Brasileira de Ciência do Solo, p 695p
Kampf N, Curi N, Marques Jr J (2009) Intemperismo e ocorrência de minerais no ambiente do solo. Química e Mineralogia do Solo, 334–379.
Klug HP, Alexander LE (1974) X-Ray diffraction procedures for polycrystalline and amorphous materials. Wiley
Kroth PL (1988) Disponibilidade de fósforo no solo para plantas e fatores que afetam a extração por resina de troca em membrana. Dissertation, Federal University of Rio Grande do Sul.
Lacerda MPC, Barbosa IO (2012) Soil-geomorphological relationships and pedoforms distribution in the ecological station of águas emendadas, Distrito Federal. Rev Bras Ciênc Solo 36:709–722. https://doi.org/10.1590/S0100-06832012000300003
Li ZW, Zhang GH, Geng R, Wang H (2015) Rill erodibility as influenced by soil and land use in a small watershed of the loess plateau China. Biosyst Eng 129:248–257. https://doi.org/10.1016/j.biosystemseng.2014.11.002
Lima HN, Mello JWV, Schaefer CEGR, Ker JC, Lima AMN (2006) Mineralogy and chemistry of three soils along a topossequence from the Upper Solimões Basin, western Amazonia. Rev Bras Ciênc Solo 30:59–68. https://doi.org/10.1590/S0100-06832006000100007

Lima JGC, Schulze SMBB, Ribeiro MR, Barreto SB (2008) Mineralogy of an Ultisol in the coastal humid zone of Pernambuco, Brazil. Rev Bras Ciênc Solo 32:881–892. https://doi.org/10.1590/S0100-06832008000200042

Marques J Jr, Lepsch IF (2000) Neo-Cenozoic superficial deposits, geomorphic surface and soils in the Monte Alto, São Paulo State. Geociências 19:265–281

Martins GC, Ferreira MM, Curi M, Vitorino ACT, Silva MLN (2006) Campos nativos e matas adjacentes da região de Humaitá (AM): atributos diferencias dos solos. Ciênc Agrotec 30:221–227. https://doi.org/10.1590/S1413-70542006000200005

McKeague JA, Day JH (1966) Dithionite and oxalate–extractable Fe and Al as aids in differentiating various classes of soils. Can J Soil Sci 46:13–22

Mehra OP, Jackson ML (1960) Iron oxide removal from soils and clay by a dithionite-citrate system buffered with sodium bicarbonate. Clays Clay Miner 7:317–327. https://doi.org/10.1346/CCMN.1958.0070122

Melo VF, Fontes MPF, Novais RF, Singh B, Schaefer CEGR (2001) Caracterização dos óxidos de ferro e de alumínio de diferentes classes de solos. Rev Bras Ciênc Solo 25:19–32. https://doi.org/10.1590/S01000683200100010003

Melo MS, Riccomini C, Hasui Y, Almeida FFM, Coimbra AM (2018) Geologia e evolução do sistema de bacias tafrogênicas continentais do sudeste do Brasil. Rev Bras Geociênc (online) 15:193–201

Miguel P, Dalmolin RSD, Pedron FA, Fink JR, Bueno JMM (2013) Plintites and petroplintites characterization in soils from central depression of the Rio Grande do Sul state, Brazil. Ciênc Rural 43:999–1005. https://doi.org/10.1590/S0103-84782013005000065

Minasny B, Mcbratney AB (2006) Mechanistic soil-landscape modelling as an approach to developing pedogenetic classifications. Geoderma 133:138–149. https://doi.org/10.1016/j.geoderma.2006.03.042

Montanari R, Marques J Jr, Campos MCC, Souza ZM, Camargo LA (2010) Characterization mineralogical of Oxisol in different relief form in the region of Jaboticabal, SP. Cienc Agron 41:191–199. https://doi.org/10.1590/S1806-66902010000200004

Murphy J, Riley JPA (1962) Modified single solution method for the determination of phosphate in natural waters. Anal Chim Acta 27:31–36. https://doi.org/10.1016/S0003-2670(00)88444-5

Neves CMN, Silva MLN, Curi N, Macedo RLG, Moreira FMS, Norrish K, Taylor RM (1961) The isomorphous replacement of iron by aluminum in soil goethites. J Soil Sci 12:294–306. https://doi.org/10.1111/j.1365-2389.1961.tb00919.x

Norrish K, Taylor RM (1961) The isomorphous replacement of iron by aluminum in soil goethites. J Soil Sci 12:294–306. https://doi.org/10.1111/j.1365-2389.1961.tb00919.x

Pinto FA, Souza ED, Paulino HB, Curi N, Carneiro MACP (2013) P-sorption and desorption in Savanna Brazilian soils as a support for phosphorus fertilizer management. Ciênc Agrotec 37:521–530. https://doi.org/10.1590/S1413-70542013000600005

Poggere GC, Inda AV, Barrón V, Kämpf N, De Brito ADB, Barbosa JZ, Curi N (2018) Maghemite quantification and magnetic signature of Brazilian soils with contrasting parent materials. Appl Clay Sci 161:385–394. https://doi.org/10.1016/j.clay.2018.05.014

Prietzel J, Klysubun W, Hurtarte LCC (2020) The fate of calcium in temperate forest soils: a Ca K-edge XANES study. Biogeochemistry 152:195–222. https://doi.org/10.1007/s10533-020-00748-6

Ribeiro MR, Oliveira LB, Araujo Filho JC, Ker JC, Curi N, Schaefer CEGR, Vidal-Tornado P (2012) Caracterização morfológica do solo. eds. In: Ker JC, Curi N, Schaefer CEGR, Vidal-Torrado P (eds) Pedologia: Fundamentos. Brazilian Society of Soil Science, pp 81–146

Rodrigues AL, Watzlawick LF, Genú AM, Hess AF, Ebling ÂA (2016) Atributos de um solo florestal em uma topossequência e relações com a comunidade arbórea. Floresta 46:145–154. https://doi.org/10.5380/rf.v46i2.36219

Rotta LR, Paulino HB, Anghinoni I, Souza ED, Carneiro MAC (2015) Phosphorus fractions and availability in a haplic plinthosol under no-tillage system in the Brazilian Cerrado. Ciênc Agrotec 39:216–224. https://doi.org/10.1590/S1413-70542015000300002

Santos AC, Pereira MG, Anjos LHC, Bernini TA, Cooper M, Nummer AR, Francelino MR (2010) Gênese e classificação de solos numa topossequência no ambiente de mar de morros do médio Vale do Paraíba do Sul, RJ. Rev Bras Ciênc Solo 34:1297–1314. https://doi.org/10.1590/S01000683201000040027

Santos LAC, Campos MCC, Costa HS, Pereira AR (2012) Caracterização de solos em uma topossequência sob terraços aluviais na região do médio rio Madeira (AM). Ambiência 8:319–331. https://doi.org/10.5777/ambiencia.2012.02.07

Santos RD, Lemos RC, Santos HG, Ker JC, Anjos LHC, Shimizu SH (2013) Manual de descrição e coleta de solos no campo, 6th edn. Brazilian Society of Soil Science

Santos HG, Jacomine PKT, Anjos LHC, Oliveira VA, Lumbreras JF, Coelho MR, Cunha TJF (2018) Sistema brasileiro de classificação de solo, 3rd edn. Embrapa

Scarciglia F, Pera E, Critelli S (2005) Weathering and pedogenesis in the Sila Grande Massif (Calabria, South Italy): from field scale to micromorphology. CATENA 61:1–29. https://doi.org/10.1016/j.catena.2005.02.00

Schiavo JA, Pereira MG, Miranda LPMD, Neto D, Hypólitom A, Fontana A (2010) Caracterização e classificação de solos desenvolvidos de arenitos da formação Aquidauana-MS. Rev Bras Ciênc Solo 3:881–889. https://doi.org/10.1590/S0100-06832010000300029

Schulze DG (1984) The influence of aluminum on iron oxides: VIII. Unit-cell dimensions of Al-substituted goethites and estimation of Al from them. Clays Clay Miner 32:36–44

Schulze DG, Schwertmann U (1984) The influence of aluminium on iron oxides: X properties of Al-substituted goethites. Clay Miner 19:521–539. https://doi.org/10.1180/claymin.1984.019.4.02

Schwertmann U, Kämpf N (1985) Properties of goethite and hematite in kaolinitic soils of Southern and Central Brazil. Soil Sci 139:344–350

Schwertmann U, Taylor RM (1989) Iron oxides. In: Dixon JB, Weed SB (eds) Minerals in soil environments. Soil Science Society of America, pp 379–438

Silva MB, Anjos LHC, Pereira MG, Nascimento RAM (2001) Estudo de topossequência da baixada litorânea fluminense: Efeitos do material de origem e posição topográfica. Rev Bras Ciênc Solo 25:965–976. https://doi.org/10.1590/S0100-06832001000400019

Silva LS, Marques J Jr, Barrón V, Gomes RP, Teixeira DDB, Siqueira DS, Vasconcelos V (2020) Spatial variability of iron oxides in soils from Brazilian sandstone and basalt. CATENA 185:104258. https://doi.org/10.1016/j.catena.2019.104258

Skogley O, Dobermann A (1996) Synthetic Ion-exchange resins: soil and envinonmental studies. J Environ Qual 25:13–24. https://doi.org/10.2134/jeq1996.00472425002500010004x

Soil Survey Staff (2014) Soil taxonomy, twelfth ed. USDA, Washington, DC. https://www.nrcs.usda.gov/wps/portal/nrcs/detail/soils/survey/class/taxonomy/?cid=nrcs142p2_053580. (Accessed 11 Sept 2021)

Sommer M (2006) Influence of soil pattern on matter transport in and from terrestrial biogeosystems - A new concept for landscape pedology. Geoderma 133:107–123. https://doi.org/10.1016/j.geoderma.2006.03.040

Tunçay T, Dengiz O (2020) The roles of parent material and toposequence on geochemical characteristics and pedogenic iron oxides of soils Indian. J Mar Sci 49:622–623

Vasconcelos V, Carvalho JAO, Martins ES, Couto Júnior AF, Guimaraes RF, Gomes RAT (2012) Geomorphometric classification

system based on a two-stage sequential architecture decision tree and spectral classifier in the Serra da Canastra National Park. Rev Bras Geomorforfol 13:171–186. https://doi.org/10.20502/rbg.v13i2.248

ZEE - Zoneamento Ecológico Econômico Do Sul-Sudeste Do Amazonas (2008) Zoneamento ecológico econômico do sul-sudeste do amazonas. IPAAM